Title: Newly identified varicella-zoster virus latency transcript inhibits viral replication

Authors: Daniel P. Depledge[1†], Werner J.D. Ouwendijk[2†], Tomohiko Sadaoka[3†], Shirley E. Braspenning[2], Yasuko Mori[3], Randall J. Cohrs[4], Georges M. G. M. Verjans[2,5‡*] and Judith Breuer[1‡*]

Affiliations:

[1]Division of Infection and Immunity, University College London, London, WC1E 6BT, United Kingdom.

[2]Department of Viroscience, Erasmus Medical Center, 3015 CN, Rotterdam, The Netherlands.

[3]Division of Clinical Virology, Center for Infectious Diseases, Kobe University Graduate School of Medicine, 7-5-1 Kusunoki-cho, Chuo-ku, Kobe, 650-0017, Japan.

[4]Department of Neurology, University of Colorado School of Medicine, Aurora, Colorado, 12700, USA; Department of Immunology & Microbiology, University of Colorado School of Medicine, Aurora, Colorado, 12800, USA.

[5]Research Center for Emerging Infections and Zoonoses, University of Veterinary Medicine Hannover, 30559, Hannover, Germany.

***Correspondence to:** Judith Breuer at the Division of Infection and Immunity, University College London, WC1E 6BT, London, United Kingdom. Phone: +44 20 3108 2130 and Email: j.breuer@ucl.ac.uk /breuej@gosh.nhs.uk and Georges M.G.M. Verjans at the Department of Viroscience, Erasmus Medical Center, 3015 CN, Rotterdam, The Netherlands. Phone: +31 10 7044066 and Email: g.verjans@erasmusmc.nl

The following authors contributed equally as first[†] (DPD, WJDO and TS) and last[‡] (GMGMV and JB) authors.

Abstract:

Varicella-zoster virus (VZV) persists in ganglia of >90% adults worldwide, reactivating in one-third to cause debilitating shingles. How VZV maintains latency remains unclear. Ultra-deep virus-enriched RNA sequencing of latently infected human trigeminal ganglia (TG) demonstrated consistent expression of a novel spliced VZV mRNA, partially antisense to VZV open reading frame 61 (ORF61). This VZV latency transcript (VLT) is expressed in human TG neurons and encodes a protein with late kinetics in productively infected cells *in vitro* and in shingles skin lesions. VLT but not the encoded protein represses expression of the viral transcriptional regulator ORF61 and inhibits productive viral infection. The unique characteristics of VLT can be exploited to develop novel intervention strategies aimed at preventing VZV latency and reactivation.

One sentence summary:

VZV latency is characterized by expression of a novel spliced protein-coding mRNA that represses ORF61 expression and inhibits lytic infection.

Main text:

Primary VZV infection typically causes varicella (chickenpox) during which the virus establishes latent infection in neurons of sensory and cranial ganglia, including trigeminal ganglia (TG), from which reactivation can cause herpes zoster (shingles), often accompanied by multiple serious neurological sequelae (*1*). Like other herpesviruses, productive VZV replication is characterised by full gene expression occurring with temporally linked immediate-early (IE), early (E) and late (L) kinetics to generate infectious virus progeny (*2*, *3*). Neurotropic alphaherpesviruses including herpes simplex virus type 1 (HSV-1) maintain latency in sensory ganglia through expression of a single transcript which represses transactivation of viral promotors, is anti-apoptotic and antagonises disruption of repressive chromatinisation of the latent genome (*4*). By contrast, the lack of appropriate experimental animal and *in vitro* models of VZV latency has prevented similar studies of VZV latency and its molecular characteristics remain unknown. Consequently, VZV latency has been studied in human TG yielding conflicting data concerning the extent of virus gene expression (*5*–*8*). Whereas viral protein detection by immunohistochemistry can largely be attributed to non-specific binding of anti-VZV antibodies (*9*, *10*), the post-mortem interval (PMI) between death and TG specimen processing determines the number of VZV transcripts detected (*11*). Using PCR primers targeting the 70 canonical VZV genes, only open reading frame 63 (ORF63) is occasionally detected in TG with PMI <9 hrs (*11*), while multiple virus transcripts of different kinetic classes are observed in human TG with PMI >9 hrs. The lytic gene ORF63 does not share the characteristics associated with other alphaherpesvirus latency transcripts (*1*).

The aim of this study was to map the latent transcriptomes of VZV and HSV-1 in co-infected human TG harvested with short PMI (≤8 hrs) using ultra-deep RNA sequencing (RNAseq), with and without targeted enrichment of viral nucleic acids (*12*). Our experimental approach was validated using lytically VZV- or HSV-1-infected human retinal pigmented

epithelial (ARPE-19) cells to demonstrate unbiased detection of all currently annotated VZV and HSV-1 genes at high specificity and sensitivity (Fig. 1A and B). Ultra-deep sequencing of unenriched RNA libraries, selected for polyadenylated transcripts (Fig. 1A) or ribosomal RNA (rRNA)-degraded total RNA (Fig. S1A), from two TG failed to identify any VZV transcripts (donors 1-2; Tables S1 and S2). However, expression of the stable 1.5/2.0 kb latency associated transcript (LAT)-derived introns, a hallmark of HSV-1 latency (*13*) was readily detected in both TG specimens (Fig 1B, Fig. S1B and Fig. S2). By contrast, targeted enrichment of seven TG (donors 1-7; Tables S1 and S2) for VZV RNA sequences revealed the presence of a novel 496 nucleotide multi-exon polyadenylated mRNA expressed partially antisense to VZV ORF61 (Fig. 1A and C). Targeted enrichment for HSV-1 RNA sequences in the same seven TG recovered both LAT introns and the near complete 8.3 kb full-length LAT transcript from which they derive, but no other transcripts (Fig. 1B and S2B). Furthermore, several latency associated miRNAs (mir-H2, mir-H3, mir-H4, mir-H6, mir-H7 and mir-H14) (*14*) were detected in two TG (donors 1 and 2) by qPCR and all of four TG (donors 1, 2, 5 and 8) by miRNA sequencing of unenriched RNA libraries (Table S1 and data not shown). Manual inspection of the VZV sequence read data, combined with *de novo* transcript reconstruction, revealed the presence of five distinct exons of which the most 3' contains a canonical polyadenylation signal site (AAUAAA) and cleavage factor I-binding motif (TGTA, Fig. 1C). We term this novel spliced transcript the VZV latency transcript (VLT). Except for ORF63 transcript in six of seven TG (donors 2-7), no other VZV transcripts or miRNAs were detected (Fig. 1C and data not shown).

To confirm these observations, TG specimens from 18 individuals (donors 1-18; Table S1) with PMI ≤8 hrs were analysed for the presence of VZV and HSV-1 DNA and transcripts by qPCR and reverse transcriptase qPCR (RT-qPCR), respectively. Thirteen TG were co-infected with VZV and HSV-1 while remaining TG contained only VZV (n=2; donors 10 and 12) or HSV-1 (n=3; donors 16 – 18), (Table S1). Fourteen of 15 (93%) VZV nucleic acid positive (VZV^{POS}) TG

expressed VLT, as detected by specific primer/probe-combinations spanning exon 2→3 and 3→4 junctions (Fig. S3) and 9 of 15 (60%) VZV^{POS} TG co-expressed ORF63 mRNA at lower levels relative to VLT (Fig. 2A and Table S1). The high correlation between VLT levels detected by both VLT primer/probe sets supported detection of a single multiply spliced transcript (Fig. 2B). VLT levels correlated significantly with ORF63 transcript levels (Fig. 2B), but not with VZV DNA load or PMI, excluding the possibility of post mortem-induced viral reactivation (Fig. S4A and B) (*11*). *In situ* hybridization (ISH) analyses of latently infected human TG (n=12 VZV^{POS} and n=10 HSV-1^{POS}) confirmed the RNASeq and RT-qPCR data (Fig. S4C), with expression of VLT (0.49% ± 0.20%; average ± SD) and ORF63 transcript (0.36% ± 0.16%) in fewer TG neurons than HSV-1 LAT (5.5% ± 3.5%) (Fig. S5). VLT and ORF63 transcripts were localized to both the neuronal nucleus and cytoplasm (Fig 2C and D), with preferential cytoplasmic expression of VLT (Fig. 2D). RNase, but not DNase treatment abolished ORF63- and VLT-specific ISH staining confirming detection of viral transcripts and not viral genomic DNA (Fig. S6).

In silico translation of the VLT sequence predicted a 137 amino acid protein (pVLT) with start codon and polyadenylation site/stop codon in exons 2 and 5, respectively (Fig. S3). A polyclonal pVLT-specific antibody, generated against the first 19 N-terminal pVLT residues, confirmed pVLT expression in the nucleus and cytoplasm of VLT-transfected, and predominantly nuclear in VZV-infected ARPE-19 cells (Fig. 3A and B). In VZV-infected ARPE-19 cells, pVLT co-localized with nuclear-expressed ORF62 protein (IE62), but not the cytoplasmically-expressed glycoprotein B (Fig. 3B). The kinetic class of VLT was determined by RT-qPCR in VZV-infected ARPE-19 cells cultured in the presence or absence of phosphonoformic acid (PFA), a broad spectrum herpesvirus DNA polymerases inhibitor (*15*). As expected, ORF61 (IE gene) and ORF29 (E gene) transcription was not affected, while ORF49 (L gene) was markedly reduced in PFA-treated VZV-infected cells (Fig. 3C). PFA blocked VLT

expression completely demonstrating that VLT transcription is dependent on viral DNA replication and occurs late during the lytic VZV replication cycle *in vitro* (Fig. 3C). Finally, herpes zoster skin biopsies were assayed for expression of VLT and pVLT by ISH and immunohistochemistry (IHC), respectively. VLT was expressed throughout the epidermis and dermis, particularly in association with skin vesicles (Fig. 3D). IHC analyses on consecutive sections for VZV ORF63 protein (IE63) and pVLT indicated co-expression in the same skin areas (Fig. 3E), which was confirmed by confocal microscopy (Fig. 3F). No pVLT-specific IHC signal was detected in latently VZV-infected human TG sections (data not shown).

HSV-1 LAT represses the expression of the immediate early ICP0 gene, thereby restricting virus replication (*16*, *17*), and promotes cell survival by inhibiting cellular susceptibility to apoptotic stimuli (*18*). By contrast, constitutive VLT expression did not protect ARPE-19 cells from apoptosis (Fig. S7). Because VLT is partially antisense to ORF61, the VZV ICP0 homologue (*19*), we determined whether VLT represses expression of ORF61 in VLT-transfected ARPE-19 cells. VLT expression significantly reduced ORF61, but not ORF62 and ORF63 transcript levels in ARPE-19 cells co-transfected with all four VZV genes (Fig. 4A). Mutation of the pVLT start codon (ATG→ATA) resulted in loss of pVLT expression in co-transfected ARPE-19 cells (Fig. 4B), but did not abolish the inhibitory effect of VLT on ORF61 transcript and protein (IE61) expression in co-transfected cells, implicating the role of VLT but not pVLT (Fig. 4). Western blot analysis confirmed that VLT diminishes IE61, but not IE63 and α-tubulin protein abundance in co-transfected ARPE-19 cells (Fig. 4B). In VZV replication assays using ARPE-19 cells, stably transfected with a plasmid encoding VLT or empty plasmid, VLT reduced the number of IE61-positive cells at eight hours post-infection with cell-free VZV (Fig. 4C), and inhibited both VZV DNA replication and virus spread at 72 hours (Fig. 4D and E). Together these data indicate the specific role of VLT in blocking ORF61 gene expression and subsequent virus replication.

In the absence of tractable experimental cell and animal models that recapitulate all features of VZV latency observed in humans (*20–22*), we used ultra-deep RNAseq to profile latent VZV in naturally infected human TG with short PMI. We have identified a novel spliced VZV transcript VLT that is consistently expressed in latently VZV-infected human TG neurons. VLT encodes a protein that is expressed with late kinetics in lytically VZV-infected cells *in vitro* and in human VZV skin lesions. Whereas the pVLT function remains to be determined, VLT RNA specifically supresses expression of VZV IE61, a homologue of HSV-1 ICP0 and a promiscuous transactivator of lytic viral promotors (*23*). Additionally, VLT may contribute to maintaining latency by limiting the function of IE61 protein as a histone deacetylase inhibitor to maintain chromatin repression of VZV gene transcription (*19*, *24*). VLT differs markedly from the well-characterized latency transcripts of other alphaherpesviruses, notably HSV-1 and bovine herpesvirus 1 (BHV-1), which are described to block apoptosis and also encode miRNAs that are responsible for downregulating expression of HSV-1 ICP0 and the BHV-1 homologue (*14*, *18*, *25*, *26*). VLT neither encodes any detectable miRNAs nor impairs apoptosis *in vitro*.

VZV is the only human herpesvirus for which commercial vaccines that effectively prevent both primary varicella and reactivation to cause shingles are licensed and in use (*27*, *28*). However, these vaccines contain the live-attenuated VZV vOka strain which establishes latency and reactivates (*29*). With the discovery of VLT and its potential role in maintaining latency, development of a novel varicella vaccine that does not establish latency or reactivate, and drugs that eradicate latent VZV, are now a realistic goal.

References and notes

1. A. M. Arvin, D. H. Gilden, in *Fields Virology*, D. M. Knipe, P. M. Howley, Eds. (Lippincott Williams & Wilkins, Philadelphia, ed. 6th, 2013), pp. 3112 – 3179.
2. M. Reichelt, J. Brady, A. M. Arvin, The replication cycle of varicella-zoster virus: analysis of the kinetics of viral protein expression, genome synthesis, and virion assembly at the single-cell level. *J. Virol.* **83**, 3904–18 (2009).
3. P. E. Pellet, B. Roizman, in *Fields Virology*, D. M. Knipe, P. M. Howley, Eds. (Lippincott Williams & Wilkins, Philadelphia, ed. 6th, 2013), pp. 2770 – 2802.
4. P. G. E. Kennedy, J. Rovnak, H. Badani, R. J. Cohrs, A comparison of herpes simplex virus type 1 and varicella-zoster virus latency and reactivation. *J. Gen. Virol.* **96**, 1581–602 (2015).
5. P. G. E. Kennedy, R. J. Cohrs, Varicella-zoster virus human ganglionic latency: a current summary. *J. Neurovirol.* **16**, 411–418 (2010).
6. R. J. Cohrs, D. H. Gilden, Prevalence and abundance of latently transcribed varicella-zoster virus genes in human ganglia. *J. Virol.* **81**, 2950–2956 (2007).
7. R. J. Cohrs, D. H. Gilden, P. R. Kinchington, E. Grinfeld, P. G. E. Kennedy, Varicella-zoster virus gene 66 transcription and translation in latently infected human Ganglia. *J. Virol.* **77**, 6660–5 (2003).
8. M. A. Nagel *et al.*, Varicella-zoster virus transcriptome in latently infected human ganglia. *J. Virol.* **85**, 2276–87 (2011).
9. L. Zerboni *et al.*, Apparent expression of varicella-zoster virus proteins in latency resulting from reactivity of murine and rabbit antibodies with human blood group a determinants in sensory neurons. *J. Virol.* **86**, 578–83 (2012).
10. W. J. D. Ouwendijk *et al.*, Immunohistochemical detection of intra-neuronal VZV proteins in snap-frozen human ganglia is confounded by antibodies directed against blood group A1-associated antigens. *J. Neurovirol.* **18**, 172–180 (2012).

11. W. J. D. Ouwendijk *et al.*, Restricted varicella-zoster virus transcription in human trigeminal ganglia obtained soon after death. *J. Virol.* **86**, 10203–6 (2012).

12. D. P. Depledge *et al.*, Specific Capture and Whole-Genome Sequencing of Viruses from Clinical Samples. *PLoS One*. **6** (2011), doi:10.1371/journal.pone.0027805.

13. J. G. Stevens, E. K. Wagner, G. B. Devi-Rao, M. L. Cook, L. T. Feldman, RNA complementary to a herpesvirus alpha gene mRNA is prominent in latently infected neurons. *Science (80-.).* **235**, 1056–1059 (1987).

14. J. L. Umbach *et al.*, MicroRNAs expressed by herpes simplex virus 1 during latent infection regulate viral mRNAs. *Nature*. **454**, 780–783 (2008).

15. Y. C. Cheng *et al.*, Mode of action of phosphonoformate as an anti-herpes simplex virus agent. *Biochim. Biophys. Acta*. **652**, 90–8 (1981).

16. N. Mador, D. Goldenberg, O. Cohen, A. Panet, I. Steiner, Herpes simplex virus type 1 latency-associated transcripts suppress viral replication and reduce immediate-early gene mRNA levels in a neuronal cell line. *J. Virol.* **72**, 5067–75 (1998).

17. M. P. Nicoll *et al.*, The HSV-1 Latency-Associated Transcript Functions to Repress Latent Phase Lytic Gene Expression and Suppress Virus Reactivation from Latently Infected Neurons. *PLoS Pathog.* **12**, e1005539 (2016).

18. G. C. Perng *et al.*, Virus-induced neuronal apoptosis blocked by the herpes simplex virus latency-associated transcript. *Science*. **287**, 1500–1503 (2000).

19. L. Wang, M. Sommer, J. Rajamani, A. M. Arvin, Regulation of the ORF61 Promoter and ORF61 Functions in Varicella-Zoster Virus Replication and Pathogenesis. *J. Virol.* **83**, 7560–7572 (2009).

20. A. Markus, I. Lebenthal-Loinger, I. H. Yang, P. R. Kinchington, R. S. Goldstein, An In Vitro Model of Latency and Reactivation of Varicella Zoster Virus in Human Stem Cell-Derived Neurons. *PLoS Pathog.* **11**, 1–22 (2015).

21. T. Sadaoka *et al.*, In vitro system using human neurons demonstrates that varicella-

zoster vaccine virus is impaired for reactivation, but not latency. *Proc. Natl. Acad. Sci.*, 201522575 (2016).

22. K. Haberthur, I. Messaoudi, Animal Models of Varicella Zoster Virus Infection. *Pathogens* (2013), doi:10.3390/pathogens2020364.
23. H. Moriuchi, M. Moriuchi, S. E. Straus, J. I. Cohen, Varicella-zoster virus (VZV) open reading frame 61 protein transactivates VZV gene promoters and enhances the infectivity of VZV DNA. *J. Virol.* (1993).
24. C. Boutell, R. D. Everett, Regulation of alphaherpesvirus infections by the ICP0 family of proteins. *J. Gen. Virol.* **94**, 465–481 (2013).
25. T. Jaber, A. Workman, C. Jones, Small Noncoding RNAs Encoded within the Bovine Herpesvirus 1 Latency-Related Gene Can Reduce Steady-State Levels of Infected Cell Protein 0 (bICP0). *J. Virol.* **84**, 6297–6307 (2010).
26. J. Ciacci-Zanella, M. Stone, G. Henderson, C. Jones, The latency-related gene of bovine herpesvirus 1 inhibits programmed cell death. *J. Virol.* **73**, 9734–40 (1999).
27. M. N. Oxman *et al.*, A Vaccine to Prevent Herpes Zoster and Postherpetic Neuralgia in Older Adults. *N. Engl. J. Med.* **352**, 2271–2284 (2005).
28. M. Takahashi *et al.*, Live Vaccine Used To Prevent the Spread of Varicella in Children in Hospital. *Lancet*. **304**, 1288–1290 (1974).
29. S. A. Galea *et al.*, The Safety Profile of Varicella Vaccine: A 10-Year Review. *J. Infect. Dis.* **197**, S165–S169 (2008).
30. T. Sadaoka, H. Yoshii, T. Imazawa, K. Yamanishi, Y. Mori, Deletion in open reading frame 49 of varicella-zoster virus reduces virus growth in human malignant melanoma cells but not in human embryonic fibroblasts. *J. Virol.* **81**, 12654–12665 (2007).
31. W. J. D. Ouwendijk *et al.*, Functional characterization of ocular-derived human alphaherpesvirus cross-reactive CD4 T cells. *J. Immunol.* **192**, 3730–9 (2014).
32. T. Lenac Roviš *et al.*, Comprehensive analysis of varicella-zoster virus proteins using a

new monoclonal antibody collection. *J. Virol.* **87**, 6943–54 (2013).

33. A. Sloutskin, P. R. Kinchington, R. S. Goldstein, Productive vs non-productive infection by cell-free varicella zoster virus of human neurons derived from embryonic stem cells is dependent upon infectious viral dose. *Virology*. **443**, 285–293 (2013).

34. D. P. Depledge *et al.*, Deep sequencing of viral genomes provides insight into the evolution and pathogenesis of varicella zoster virus and its vaccine in humans. *Mol. Biol. Evol.* **31**, 397–409 (2014).

35. M. Krzywinski *et al.*, Circos: An information aesthetic for comparative genomics. *Genome Res.* **19**, 1639–1645 (2009).

36. K. Rutherford *et al.*, Artemis: sequence visualization and annotation. *Bioinformatics*. **16**, 944–945 (2000).

37. I. Milne *et al.*, Tablet-next generation sequence assembly visualization. *Bioinformatics*. **26** (2009), pp. 401–402.

38. M. G. Grabherr *et al.*, Full-length transcriptome assembly from RNA-Seq data without a reference genome. *Nat. Biotechnol.* **29**, 644–52 (2011).

39. M. van Velzen *et al.*, Longitudinal study on oral shedding of herpes simplex virus 1 and varicella-zoster virus in individuals infected with HIV. *J. Med. Virol.* **85**, 1669–77 (2013).

40. J. Schindelin *et al.*, Fiji: an open-source platform for biological-image analysis. *Nat. Methods* (2012), doi:10.1038/nmeth.2019.

41. T. Sadaoka *et al.*, Varicella-Zoster Virus ORF49 Functions in the Efficient Production of Progeny Virus through Its Interaction with Essential Tegument Protein ORF44. *J. Virol.* **88**, 188–201 (2014).

42. Y. Hama *et al.*, Antibody to varicella-zoster virus immediate-early protein 62 augments allodynia in zoster via brain-derived neurotrophic factor. *J. Virol.* **84**, 1616–24 (2010).

43. T. Okuno, K. Yamanishi, K. Shiraki, M. Takahashi, Synthesis and Processing of Glycoproteins of Varicella-Zoster Virus (VZV) as Studied with Monoclonal Antibodies to

VZV Antigens. *Virology*. **129**, 357–368 (1983).

44. P. G. Kennedy, E. Grinfeld, S. Bontems, C. Sadzot-Delvaux, Varicella-Zoster virus gene expression in latently infected rat dorsal root ganglia. *Virology*. **289**, 218–23 (2001).

45. W. J. D. Ouwendijk *et al*., T-Cell Tropism of Simian Varicella Virus during Primary Infection. *PLoS Pathog.* **9** (2013), doi:10.1371/journal.ppat.1003368.

Acknowledgements

DPD is supported by a New Investigator Award from the Medical Research Foundation (UK MRC) and a small grant provided by the Daiwa Foundation. JB was partially funded by the UCL/UCLH Biomedical Research Centre (BRC). TS received funding from the Takeda Science Foundation, Japan Society for the Promotion of Science (JSPS KAKENHI JP17K008858) and the Ministry of Education, Culture, Sports, Science and Technology (MEXT KAKENHI JP17H05816) and was, in part, supported by a Grant-in-Aid for Scientific Research on Innovative Areas from MEXT of Japan (JP16H06429 and JP16K21723). WJDO, RJC and GMGMV were partly supported by National Institutes of Health grant AG032958. GMGMV received funds from the Niedersachsen-Research Network on Neuroinfectiology (N-RENNT) of the Ministry of Science and Culture of Lower Saxony (Germany). RJC was additionally supported by Public Health Service grant NS082228. We acknowledge support from the Medical Research Council and BRC for the UCL/UCLH Pathogen Sequencing Pipeline as well as the UCL Legion High Performance Computing Facility, and associated support services, in the completion of this work. The authors would like to acknowledge Sarah Getu and Suzanne van Veen for technical assistance (Dept. of Viroscience, Erasmus MC, Rotterdam, The Netherlands) and the whole team of the Netherlands Brain Bank (www.brainbank.nl) for their work and contributions.

List of Supplementary Materials

Materials and Methods

Table S1 – S2

Fig S1 – S7

References (30 – 45)

Figure Legends

Fig. 1. Lytic and latent VZV and HSV-1 transcriptomes. Circos plots depicting VZV and HSV-1 genomes in their canonical orientation with internal tracks revealing the lytic and latent transcriptomes as determined by stranded mRNA-Seq performed with or without SureSelect target enrichment for VZV and HSV-1 nucleic acid (*viral genome*: purple band; sense ORFs, red blocks; antisense ORFs, blue blocks; latency-associated transcript of HSV-1, green blocks. (**A**) The lytic VZV transcriptome in productively infected ARPE-19 cells (left) determined by deep sequencing of VZV-enriched (black tracks) and unenriched (grey tracks) libraries. The latent VZV transcriptome in human trigeminal ganglia (TG) could not be determined in unenriched libraries (n=2, center), but demonstrates a consistent transcription pattern when sequencing VZV-enriched libraries (n=7, right). (**B**) The lytic HSV-1 transcriptome in productively infected ARPE-19 cells (left) determined by deep sequencing of HSV-1-enriched (black tracks) and unenriched (grey tracks) libraries. The latent HSV-1 transcriptome in human trigeminal ganglia (TG) in unenriched libraries (n=2, center), and enriched libraries (n=7, right).
(**A** and **B**) The Y-axis is scaled to maximum read depth per library in all cases and the newly identified VZV latency transcript (VLT) is shown in the pink box. (**C**) mRNA-Seq read data presented in a pileup format across the VZV VLT region (sense strand, 95,000 - 113,000 bp) for each of the enriched VZV transcriptomes from TG (n=7, black tracks) and productively-infected ARPE-19 cells (grey track). Previously described VZV ORFs within this locus (grey arrows), iterative repeat regions (black boxes) and the five VLT exons (blue boxes) are scaled representatively.

Fig. 2. Prevalence of VZV ORF63 transcript and VLT in human TG. (**A and B**) Relative numbers of VZV ORF63 transcript and VLT in fifteen VZV^{POS} human TG determined by reverse transcription-linked quantitative PCR (RT-qPCR). VLT2-3 and VLT3-4 refer to primers/probes spanning the junctions between VLT exons 2-3 and 3-4 respectively (Fig. S3). (**A**) Quantification

of paired ORF63 transcript and VLT levels in the same TG specimens. *** $p < 0.001$; Wilcoxon signed rank test. (**B**) RT-qPCR determined correlations between relative ORF63 transcript and VLT levels identified with VLT2-3 (left) and VLT3-4 (right) specific primer/probe pairs. Spearman correlations are indicated. Relative transcript levels: $2^{-(\text{Ct-value VZV gene} - \text{Ct-value } \beta\text{-actin})}$. (**C** and **D**) Analysis of VZV ORF63 transcript and VLT expression in twelve VZV latently infected human TG by *in situ* hybridization. (**C**) Representative images of *in situ* hybridization analysis on human TG sections using probes specific for VZV ORF63 and VLT. Magnification: 400X, Inset: 400X magnification and 3X digital zoom. (**D**) Left panel, frequency of neurons expressing VZV ORF63 and VLT in consecutive TG sections of the same donor. Middle and right panels, analysis of nuclear and cytoplasmic ORF63 and VLT expression, per TG section, in paired data from individual donors. * $p<0.05$; paired Student's t-test. ns, not significant: $p>0.05$; paired Student's t-test.

Fig. 3. Expression and localization of VLT protein *in vitro* and *in vivo*. (**A**) Confocal microscopy image of ARPE-19 cells at 48 hrs post-transfection with C-terminal FLAG-tagged VLT (pVLT-FLAG) expression plasmid. pVLT-FLAG was detected with mouse anti-FLAG (red) and rabbit anti-pVLT (green) antibodies. (**B**) Confocal microscopy images of VZV strain pOka-infected ARPE-19 cells at five days post-infection, stained for pVLT (green) and VZV ORF62 protein (IE62; red) (left panel) or pVLT (green) and VZV glycoprotein B (gB; red) (right panel). (**A** and **B**) Nuclei were stained with Hoechst 33342 (blue). Magnification: 100X and 2X digital zoom. Representative images shown for replicate independent experiments. (**C**) Analysis of VZV ORF61 (IE), ORF29 (E), ORF49 (L) transcripts and VLT levels in VZV pOka-infected ARPE-19 cells cultured in the presence or absence of phosphonoformic acid (PFA) for 24 hrs. Data represent average ± SEM from four independent experiments. (**D**) Detection of VLT expression (red) in a human herpes zoster skin lesion by *in situ* hybridization. Magnification: 100X. (**E**) Consecutive skin sections stained for ORF63 protein (IE63; brown) and pVLT (brown)

using immunohistochemistry. Magnification: 200X. (**F**) Confocal microscopy image showing co-expression of IE63 (green) and pVLT (red) within the same cells of a zoster vesicle. Nuclei were counterstained with 4',6'diamidine-2'phenylindole dihydrochloride (DAPI; blue). Magnification: 100X. (**D** to **F**) Representative images from one of two human herpes zoster skin biopsies analysed are shown.

Fig. 4. VLT selectively represses ORF61 gene expression and VZV replication *in vitro*. ARPE-19 cells were transfected with plasmids encoding FLAG-tagged VLT (VLT_{ATG}), mutated VLT in which the ATG start codon was replaced by ATA sequence (VLT_{ATA}) or empty control plasmid (empty), in combination with plasmids encoding ORF61, ORF62 and ORF63. (**A**) Expression of VZV ORF61, ORF62, ORF63 and human β-actin transcripts by RT-qPCR. *** $p < 0.001$; One-way ANOVA with Bonferroni's correction for multiple comparisons. Data represent average ~~values~~ ± SEM of two independent experiments performed in duplicate. Relative transcript levels were determined as follows: $2^{-(\text{Ct-value VZV gene} - \text{Ct-value β-actin})}$ and noting that β-actin transcription did not vary with VLT transfections nd: not detected. (**B**) Western blot analysis using rabbit antibodies to detect VZV ORF61 protein (IE61) and ORF63 proteins (IE63), or mouse antibodies to detect FLAG-tagged pVLT and α-tubulin proteins. None: untransfected ARPE-19 cells. (**C** to **E**) Polyclonal stable ARPE-19 cell lines were generated by transfection of cells with plasmids encoding VLT (ARPE-VLT) or empty control plasmid (ARPE-empty), followed by >8 weeks of geneticin selection. (**C**) Confocal microscopy images showing VZV IE61 (green) in VZV strain EMC1-infected ARPE-19-empty (left) and ARPE-VLT (center) cells at 8 hrs post-infection (hpi). DAPI was used to visualize nuclei (blue). Magnification: 200X. Arrowheads indicate IE61-positive cells. Representative images are shown for replicate independent experiments (left panel). Right panel: data represent average ± SEM of replicate independent experiments, performed in triplicate. ** $p< 0.01$; unpaired Student's t-test (**D**) Analysis of VZV genome-equivalent copy numbers in VZV strain EMC-1-infected ARPE-empty

and ARPE-VLT cells at 48 hpi by qPCR. Data represent average ± SEM from replicate experiments, each performed in triplicate. ** $p < 0.01$; Mann-Whitney U test. (**E**) Virus plaque size and number in VZV-infected ARPE-empty and ARPE-VLT cells at 72 hpi. Data represent average ± SEM from replicate independent experiments, each performed in triplicate. *** $p < 0.001$; unpaired Student's t-test.

Fig. S1. The latent transcriptomes of VZV and HSV-1 profiled using rRNA-degraded libraries. Circos plots depicting the VZV and HSV-1 genomes in their canonical orientations with internal tracks revealing the latent transcriptomes as determined using rRNA-degraded sequencing libraries. (**A**) The latent VZV transcriptomes in unenriched (left) and enriched (right) libraries and (**B**) the latent HSV-1 transcriptomes in unenriched (left) and enriched (right) libraries. All libraries were all generated from the same RNA isolated from the two human TG used in the preparation of libraries detailed in Fig.1A. All figure components are as described in Figure 1.

Fig. S2. Lytic and latent transcriptomes of HSV-1.

mRNA-Seq read data presented in a pileup format across the HSV-1 LAT region (sense strand, 118,000 - 128,000 bp) for each of the enriched HSV-1 transcriptomes from TG (n=7, black tracks) and productively-infected ARPE-19 cells (grey track). Previously described HSV-1 ORFs within this locus (grey blocks), miRNAs (orange blocks), LAT-encoded ORFs (green blocks), LAT-encoded small RNAs (red blocks) and LAT (blue boxes) are scaled representatively.

Fig. S3. The VZV genomic locus encoding the VZV latency transcript. (**A**) Schematic diagram showing the genomic location (extreme 3' end of the U_L region) and structure of VLT exons (tall blocks) and introns (narrow blocks) and VZV ORF60, ORF61 and ORF62 within the genomic region 101,000 - 106,000 (co-ordinates refer to VZV reference strain Dumas). (**B**)

Location of VLT-specific primers (black arrows) and exon junction-spanning probes (yellow boxes) that recognize only the mature spliced VLT. VLT2-3 and VLT3-4 refer to primers/probes spanning the VLT exon 2→3 and 3→4 junctions, respectively.

Fig. S4. Detection of VZV ORF63 transcript and VLT, and HSV-1 LAT, in human TG. (**A** and **B**) Correlation between VZV DNA load (**A**) and post-mortem interval (PMI; **B**) and relative VZV transcript levels by qPCR in 15 VZV^{POS} human TG. Spearman r- and p-values are indicated. (**C**) Comparative analysis of HSV-1 LAT and VZV ORF63 transcript and VLT levels in 13 HSV-1/VZV co-infected human TG by qPCR. VLT2-3 and VLT3-4 indicate primer/probe sets spanning VLT exons 2→3 and 3→4 junctions, respectively. *** $p < 0.001$; Wilcoxon signed rank test.

Fig. S5. Detection of HSV-1 LAT in human TG. Analysis of HSV-1 LAT in ten latently infected human TG by *in situ* hybridization (ISH). (**A**) Representative images of ISH analysis on human TG sections using probes specific for HSV-1 LAT. (**B**) Frequency of neurons expressing HSV-1 LAT (left panel) and the frequency of neurons expressing LAT in both TG neuronal nucleus and cytoplasm compared to neurons expressing solely nuclear LAT in the same TG section (right panel). Horizontal line and error bars indicate average ± SEM.* $p<0.05$; paired Student's t-test.

Fig. S6. VLT-specific probe detects viral RNA, but not DNA in human trigeminal ganglia by *in situ* hybridization. (**A**) Analysis of negative control (bacterial gene dihydrodipicolinate reductase, DapB) and positive control (human gene RNA polymerase II polypeptide A, Polr2a) transcripts in human TG by *in situ* hybridization (ISH). Magnification: 400X. (**B**) Correlation between the percentages of VLT and ORF63 transcript positive neurons in human TG, determined by ISH. Spearman correlation $r=0.52$ and $p=0.08$. (**C**) Analysis of ISH probe

specificity using untreated, DNase-treated or RNase-treated consecutive sections of human TG. Magnification: 200X (Polr2a) and 400X (VLT). Arrowheads indicate the same neuron in adjacent TG sections. Representative images from two donors (n=2 sections/donor) are shown.

Fig. S7. Mature VLT does not inhibit apoptosis. Proportion of dead ARPE-19 cells, stably transfected to express VLT (black bars) or an empty vector control (grey bars), upon 24 hrs stimulation with medium, dimethyl sulfoxide (DMSO; 1:50), etoposide (33 µM) or apoptosis activator 2 (AA2; 100 µM) and subsequently analysed by flow cytometry. Data represent average ± SEM from replicate experiments performed in triplicate.

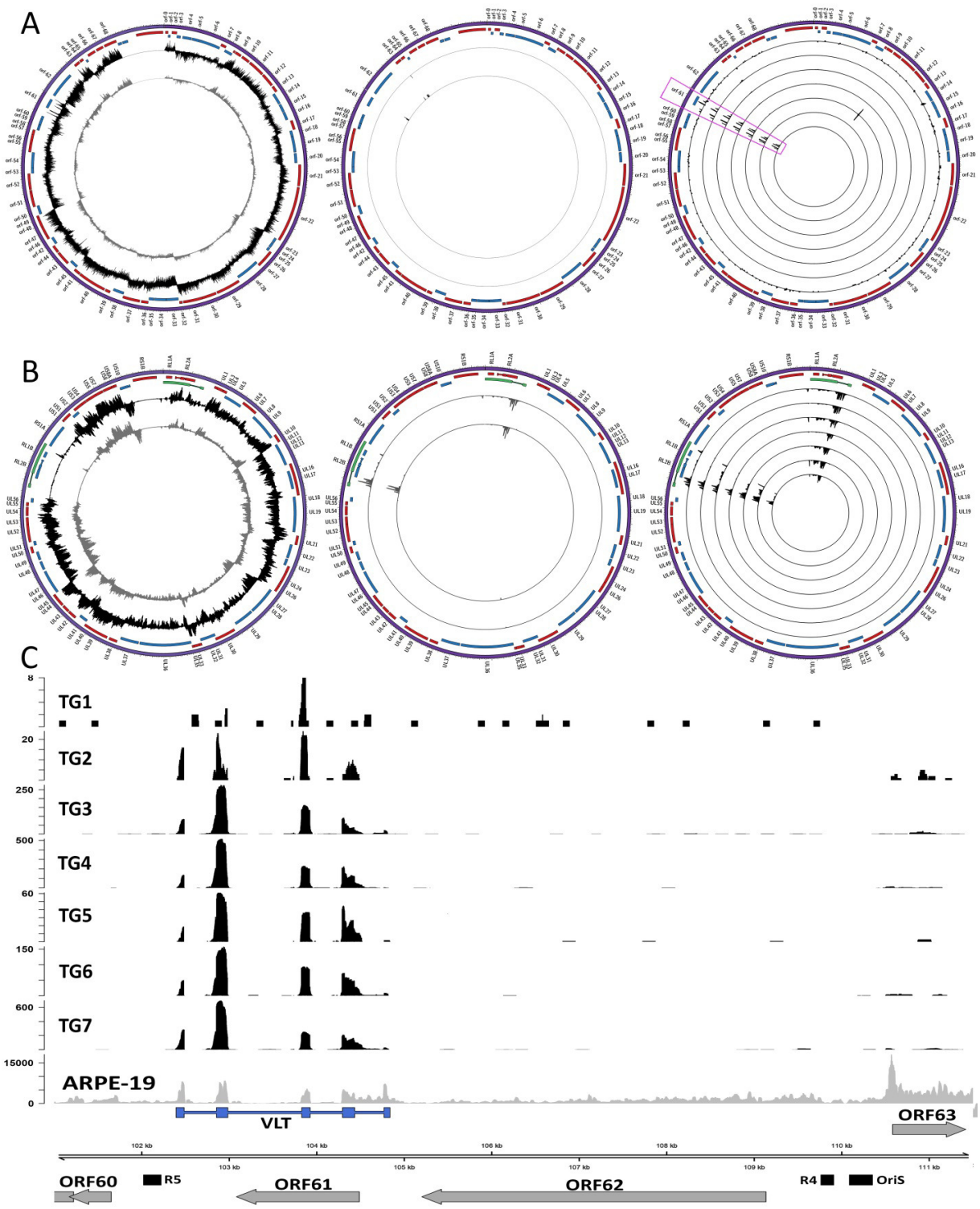
A
B
C
TG1
TG2
TG3
TG4
TG5
TG6
TG7
ARPE-19
VLT
ORF63
ORF60
R5
ORF61
ORF62
R4
OriS

Figure 1:

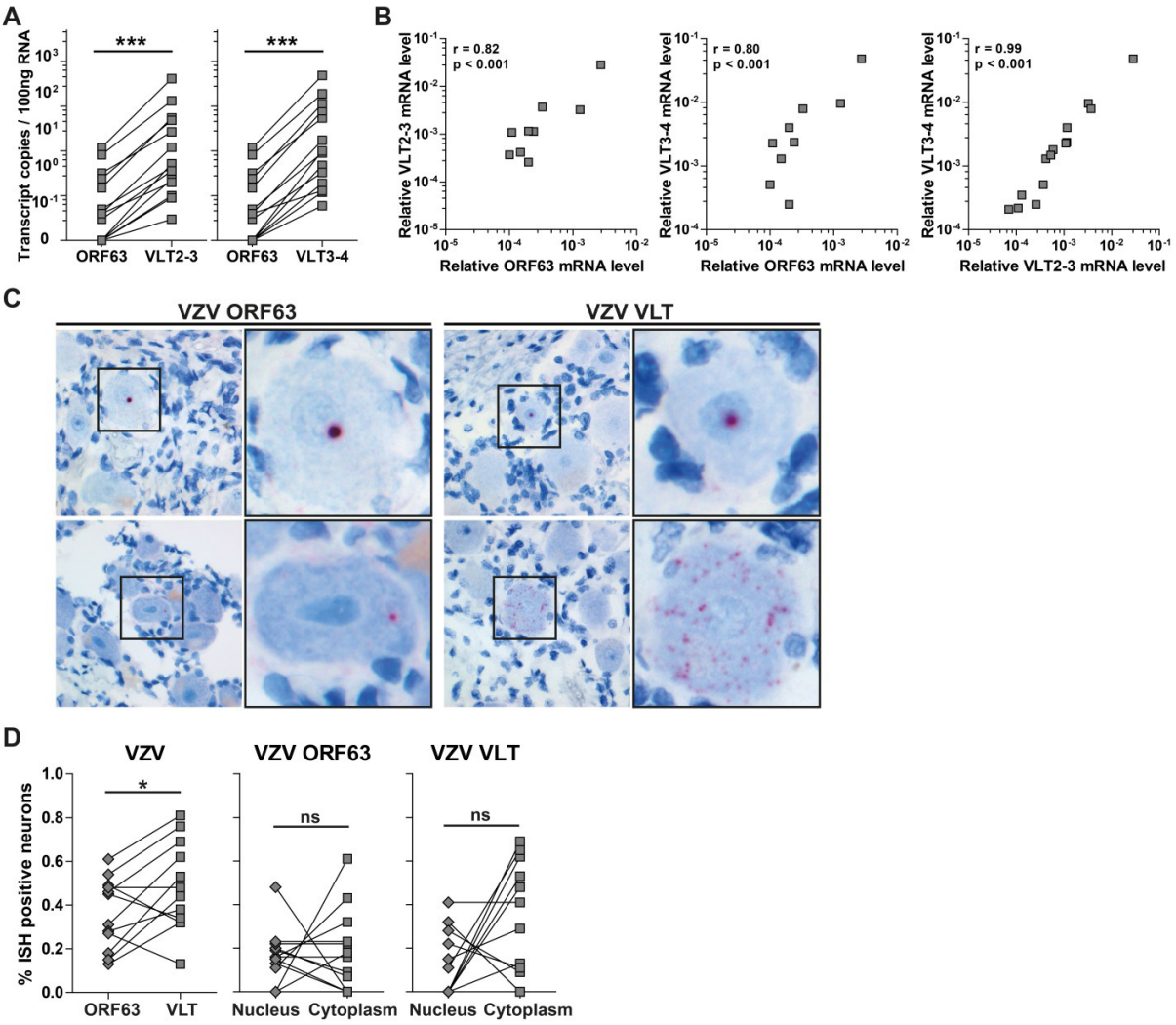
A
Transcript copies / 100ng RNA
***
***
ORF63
VLT2-3
ORF63
VLT3-4
B
Relative VLT2-3 mRNA level
r = 0.82
p < 0.001
Relative ORF63 mRNA level
Relative VLT3-4 mRNA level
r = 0.80
p < 0.001
Relative ORF63 mRNA level
Relative VLT3-4 mRNA level
r = 0.99
p < 0.001
Relative VLT2-3 mRNA level
C
VZV ORF63
VZV VLT
D
VZV
VZV ORF63
VZV VLT
% ISH positive neurons
*
ns
ns
ORF63
VLT
Nucleus
Cytoplasm
Nucleus
Cytoplasm

Figure 2:

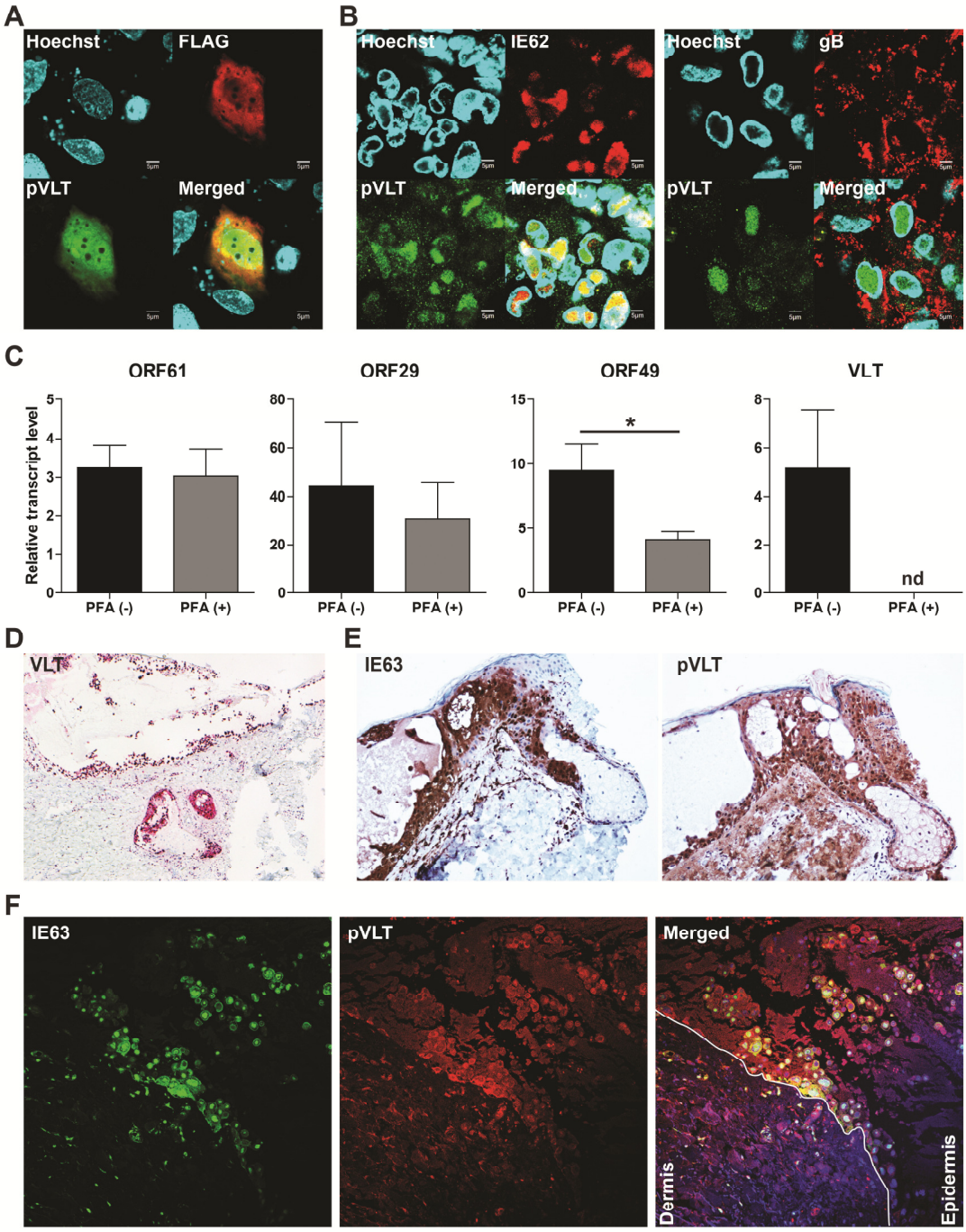
A
Hoechst
FLAG
pVLT
Merged
B
Hoechst
IE62
pVLT
Merged
Hoechst
gB
pVLT
Merged
C
ORF61
ORF29
ORF49
VLT
Relative transcript level
PFA (-)
PFA (+)
*
nd
D
VLT
E
IE63
pVLT
F
IE63
pVLT
Merged
Dermis
Epidermis

Figure 3:

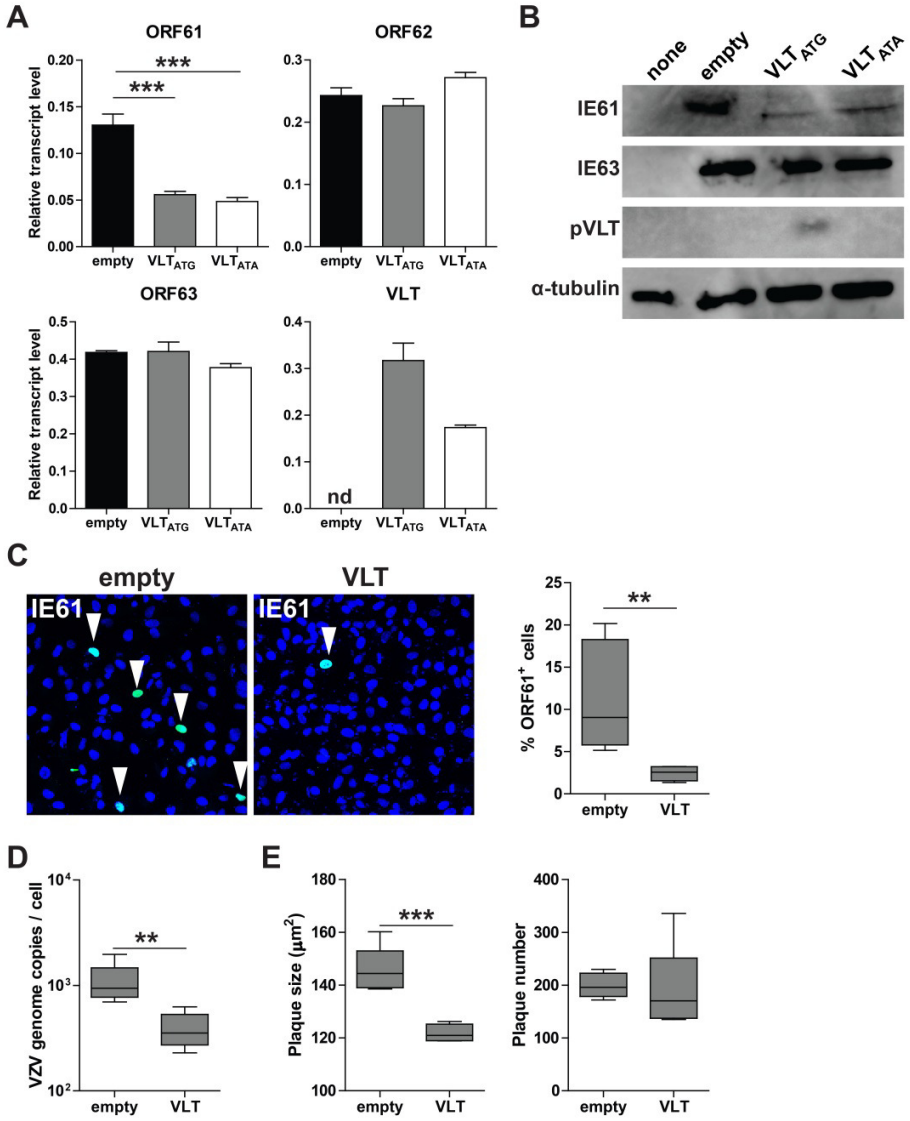
A
ORF61
ORF62
ORF63
VLT
Relative transcript level
empty
VLTATG
VLTATA
nd
B
none
empty
VLTATG
VLTATA
IE61
IE63
pVLT
α-tubulin
C
empty
VLT
IE61
% ORF61+ cells
D
VZV genome copies / cell
E
Plaque size (μm2)
Plaque number

Figure 4: